Journal of Sound and Vibration 541 (2022) 117306

Contents lists available at ScienceDirect

Journal of Sound and Vibration

journal homepage: www.elsevier.com/locate/jsvi

Acoustic radiation characteristics of cutoff modes from ducts

B. Baddour [a,*,1], P. Joseph [a,2], A. McAlpine [a,3], R. Leung [b,4]

[a] Institute of Sound and Vibration Research, Southampton, SO17 1BJ, United Kingdom
[b] Defense Science and Technology Laboratory, Fareham, PO17 6AD, United Kingdom

ARTICLE INFO

Keywords:
Duct
Modal
Radiation
Cutoff
Acoustic

ABSTRACT

The acoustic radiation from a source inside a hard-walled semi-infinite duct or tube, such as for ducted fans and rotors, is investigated. In particular a study of cutoff modes, which have the potential to affect the far-field pressure radiation for sources close to the duct open end, is presented. A large amount of work has been done to mathematically and experimentally investigate propagating cuton acoustic modes. However, there is very little published work on the radiation of cutoff modes. This paper concerns the radiation characteristics of cutoff modes to determine their behaviour, and their likely influence in the far-field directivity for sources close to the duct open end. It is shown that cutoff modes are an essential contributor for the radiation in the rear-arc.

1. Introduction

Propellers and rotors are often ducted to improve their efficiency and to enhance their safety. The sound from a number of other, often aerodynamic, sources are able to propagate to large distances via ducting systems such as ventilation ducts and exhaust ducts, before radiated to the far-field. In nearly all studies of the radiation from ducted sources the source is assumed to be buried deep inside the duct so that the effect on the radiated field due to cutoff modes can be neglected. This paper presents a fundamental investigation into the characteristics of the radiation due to cutoff modes. These modes are clearly important to the radiated field for sources that are located near the duct open end compared to the acoustic wavelength, or at frequencies just below their cutoff frequencies when their radiation efficiency is still comparatively high. In this paper, it is demonstrated that whilst cutoff modes can generally be neglected in multi-mode calculations in the forward-arc, the cutoff modes can be dominant in the rear-arc where they radiate more strongly.

1.1. Previous work

The first attempt at predicting the characteristics of ducted radiation was by Levine and Schwinger in 1948 [1] who developed the solution for the far-field acoustic pressure due to the plane wave radiating from a cylindrical hard-walled unflanged duct. The extension to higher order modes was undertaken by Tyler and Sofrin [2] in 1962. Their solution was obtained from the Kirchhoff approximation and therefore explicitly assume the existence of an infinite flange. Tyler and Sofrin's solution, while valid for both

* Corresponding author.
E-mail addresses: b.baddour@soton.ac.uk (B. Baddour), pfj@isvr.soton.ac.uk (P. Joseph), am@isvr.soton.ac.uk (A. McAlpine), R.E.Leung@soton.ac.uk (R. Leung).
[1] Post Graduate Researcher.
[2] Professor of Engineering Acoustics.
[3] Associate Professor.
[4] Principal Engineer.

https://doi.org/10.1016/j.jsv.2022.117306
Received 1 June 2022; Received in revised form 20 August 2022; Accepted 13 September 2022
Available online 17 September 2022

Nomenclature

a	Duct radius
P_{mn}	Pressure amplitude
c_0	Ambient speed of sound
D	Polar directivity (non-dimensional)
K^+, K^-	Wiener–Hopf Kernel functions
k	Acoustic wavenumber
k_z	Axial wavenumber
p	Acoustic pressure
S	Cross-sectional area
t	Time
u	Velocity
c_θ	Azimuthal phase velocity
U_{mn}	Velocity amplitude
W	Acoustic power

Coordinates:

(R, ϕ, θ)	Spherical polar coordinates
(r, θ, z)	Cylindrical polar coordinates
(x, y, z)	Cartesian coordinates
$\boldsymbol{X}$	Vector of coordinates

Greek symbols:

κ	Transverse wavenumber
ρ_0	Mean density
τ	Efficiency
η	Efficiency ratio of forward-arc to total radiation
Ψ	Shape function
ψ	Shape function in the radial dimension
ω	Angular frequency

Subscripts:

F	Flanged formulation
m	Azimuthal order
n	Radial order

propagating and non-propagating (cutoff) modes is not valid in the rear-arc and is known to be inaccurate in the sideline directions. The more general solution for the radiation from higher order modes for unflanged ducts was obtained shortly after in 1969 by Weinstein using the Wiener–Hopf method [3] whose solution was expressed in terms of complex contour integrals.

Homicz and Lordi [4] also developed an expression for the far-field modal pressure from a semi-infinite hard-walled unflanged duct using the Wiener–Hopf technique, but in a form much more amenable to computation. Mean-flow effects were included by the use of a Lorentz transformation. Subsequently, Munt [5] obtained a more general formulation for the modal radiation from circular ducts in the presence of realistic flow profiles in the duct, such as a radially varying mean flow, density and temperature. The effect on the radiation due to a centre body were included in the analysis by Gabard and Astley [6]. These additional features improved the practical capability of the unflanged duct model making it more directly applicable to aircraft engine bypass ducts.

The theoretical model of Homicz and Lordi [4] was compared to experimental data by Snakowska [7]. Snakowska compared the far-field directivity factor for a multi-modal scenario calculated using the mathematical model and using an experiment. Snakowska found that the two models were in "good accordance".

Sources located near the open end of ducts have the potential to cause non-propagating waves, known as cutoff modes, to radiate. None of these formulations directly address the distinct radiation characteristics of cutoff modes, which in this paper it is shown are fundamentally different from propagating cuton modes. Morfey [8] in 1968 has studied directly the radiation behaviour of cutoff modes, and this was confined to an analysis of their radiation efficiencies τ_{mn} from a flanged duct. He found that cuton modes radiate with near perfect (unity) radiation efficiency, but then decreases as the excitation frequency is reduced below their cuton frequency as $\tau_{mn} \propto (ka)^{2m+2}$, where m is the azimuthal order of the mode. It is noted that the rate of decay in radiation efficiency with non-dimensional (Helmholtz) frequency (ka) is independent of the radial order n of the mode. An explanation for this finding is discussed in detail in this paper.

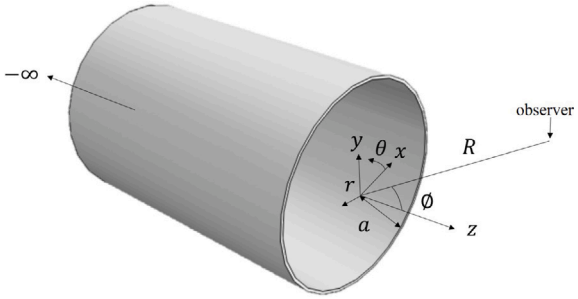

Fig. 1. Semi-infinite, hard walled unflanged duct and associated coordinate system.

The work conducted by Morfey [8] was subsequently developed by Doak [9], who repeated the analysis regarding modal radiation efficiency above and below cutoff for a finite length duct with a spherical flange. Doak noted the oscillatory behaviour of the radiation efficiency of modes excited below cutoff for modes of radial order greater than unity. Neither Doak or Morfey investigated the radiation efficiency of modes using an unflanged duct model. Similarly, they only investigated the radiation for modes that were just below cutoff.

Wang and Tszeng [10] investigated the reflection of modes from a finite length duct, although not a major feature in their work, this study included modes below cutoff. They noted that the effect of reflection for modes that are well cutoff is small, but just below cutoff it is larger.

Cutoff modes were recently studied by Snakowska and Jurkiewicz [11] who analysed the multi-modal sound field in a duct. They studied the propagation and transmission loss from cuton and cutoff modes, which can be used in muffler design. Their formulation presented a new scattering matrix computational method and incorporate near-field effects. Their predictions of the scattering matrix were compared against published results.

The distance between the source and the end of the duct was briefly investigated by Howe [12]. Howe's work is the only published study that specifically looks into the effect of locating a source at varying axial locations in a duct. Howe derived expressions for the radiated pressure field for blade vortex interaction tones of rotors located a short distance from the end of the duct. He found high and low frequency asymptotic approximations. Howe did not break the source into cuton and cutoff modal components, meaning his approach is difficult to generalise.

1.2. Scope of the investigation

In this paper a numerical study on the radiation characteristics of cutoff modes from semi-infinite, hard-walled, circular ducts in the absence of mean flow is presented. The aim is to better understand the behaviour of cutoff modes, and to highlight their fundamental differences from cuton propagating modes. The far-field modal directivity predicted using the mathematical formulation due to Gabard and Astley [6] is used as the basis for this investigation, which readily allows the prediction of the radiation from cutoff modes unlike that due to Homicz and Lordi [4] which explicitly assumes cuton modes.

This paper is divided into three parts. The first part is a study of the factors that determine the angular location of the mainlobes and sidelobes of modal radiation directivity patterns. The second part is an investigation into the radiation efficiency of cutoff modes. The third part provides a physical interpretation of the radiation characteristics of cutoff modes. In this paper it is concluded that cutoff modes generally may be disregarded in predicting forward-arc radiation, however, they can be significant in the rear-arc, and in many cases more important than the contribution from the cuton modes.

2. Acoustic radiation from a semi-infinite duct with no flow

In this section the main theoretical relationships describing the propagation and radiation of duct modes in a circular hard-walled duct are summarised. Note that mean flow is neglected in this analysis. Therefore this work is particularly relevant to marine applications where flow speeds are relatively small, but in general the work is less applicable to aerospace applications. The inclusion of mean flow is readily incorporated into the solutions, but does not alter the main conclusions and findings of this paper.

2.1. Acoustic pressure inside a duct

Consider a semi-infinite, hard-walled, unflanged duct of radius a, and cross sectional area S, as shown in Fig. 1.

The solution for the acoustic pressure within the duct is expressed in a cylindrical polar coordinate system whose origin is situated on the centre-line at the end of the duct. The duct axis is assumed to be along the z direction pointing outwards so that within the duct $z \leq 0$. Far-field observers are indicated in a spherical coordinate system at radius R, azimuthal angle θ and polar angle ϕ. The azimuthal position is in the θ-direction measured anticlockwise from the x-axis, and the polar coordinate is in the ϕ-direction

measured from the z-axis. The general form of the solution for the $(m,n)^{\text{th}}$ mode propagating along the duct can be found from separable solutions to the Helmholtz equation, at a single frequency ω, where an $\exp(-j\omega t)$ dependence is assumed. Expressed in a cylindrical coordinates system with hard walled boundary condition imposed, the modal solution is of the form,

$$\hat{p}_{mn}(r,\theta,z) = P_{mn}\Psi_{mn}(r,\theta)\,e^{jk_{z,mn}z}, \qquad z \le 0, \quad r \le a \tag{1}$$

$$\hat{u}_{mn}(r,\theta,z) = U_{mn}\Psi_{mn}(r,\theta)\,e^{jk_{z,mn}z}, \qquad z \le 0, \quad r \le a \tag{2}$$

where $\hat{p}_{mn}$ and $\hat{u}_{mn}$ are the complex pressure and axial velocity, respectively. The modal pressure amplitude is P_{mn} and the modal axial velocity amplitude is U_{mn}. Also, $\Psi_{mn}(r,\theta)$ is the normalised mode shape function, and $k_{z,mn}$ is the modal axial wavenumber. The normalised mode shape function for a circular duct is of the form [13]

$$\Psi_{mn}(r,\theta) = \psi_{mn}(r)e^{-jm\theta}, \tag{3}$$

where

$$\psi_{mn}(r) = \frac{J_m(\kappa_{mn}r)}{\sqrt{\left(1-\frac{m^2}{\kappa_{mn}^2a^2}\right)}J_m(\kappa_{mn}a)}, \tag{4}$$

and J_m is the Bessel function of the first kind of order m. The value of the modal radial wavenumber, κ_{mn}, is chosen to satisfy the hard-walled boundary condition such that $J'_m(\kappa_{mn}a) = 0$, where the prime signifies differentiation with respect to argument. Note that these mode shape function are defined to have the normalisation property $1/S\int_S|\Psi_{mn}(r,\theta)|^2dS = 1$.

Substituting the modal solution of Eq. (1) back into the wave equation leads to the dispersion relation,

$$k_{z,mn}^2 + \kappa_{mn}^2 = k^2. \tag{5}$$

This result delineates the range of propagating cuton modes $k \ge \kappa_{mn}$, from non-propagating cutoff modes $k \le \kappa_{mn}$, which is the subject of this paper. Two commonly used non-dimensional measures of the degree to which a mode is cuton or cutoff are adopted in this paper. The modal cutoff ratio ζ_{mn} is defined as,

$$\zeta_{mn} = \frac{ka}{\kappa_{mn}a}. \tag{6}$$

Cuton modes are therefore associated with $\zeta_{mn} > 1$, while cutoff modes are associated with $\zeta_{mn} < 1$.

Similarly, we define another non-dimensional index of the degree to which a mode is cuton defined by,

$$\xi_m = \frac{ka}{m}, \tag{7}$$

which will be shown to be important when considering certain characteristics of cutoff modes. Noting that $\kappa_{m,1}a \approx m$, the two modal indices are approximately related by,

$$\xi_m \approx \zeta_{m,1}\,. \tag{8}$$

2.2. Far-field pressure radiation

The far-field acoustic pressure for the mode (m,n) can be expressed in spherical coordinates of the form,

$$\hat{p}_{mn}(R,\phi,\theta) = P_{mn}\left(\frac{a}{R}\right)D_{mn}(\phi,ka)\,e^{j(kR+m\theta)} \qquad z > 0, \tag{9}$$

where $D_{mn}(\phi,ka)$ is a non-dimensional far-field modal directivity function which describes the variation in pressure with polar angle ϕ at a prescribed frequency. The directivity pattern is dependent on the non-dimensional frequency ka. Following the Wiener–Hopf equation solution by Gabard and Astley [6], the far-field modal directivity function for a semi-infinite, circular, hard-walled unflanged duct has the form,

$$D_{mn}(\phi,ka) = \frac{(ka+k_{z,mn}a)(1-\cos\phi)}{\pi(k_{z,mn}a-ka\cos\phi)ka\sin\phi H'_m(ka\sin\phi)\sqrt{\left(1-\frac{m^2}{\kappa_{mn}^2a^2}\right)}}\frac{K_m^-(\kappa_{mn}a)}{K_m^+(\cos\phi)}, \tag{10}$$

where H_m is the Hankel function of the first kind of order m, and K_m^+, K_m^- are Kernel functions of the solution discussed in Appendix. This solution is valid at frequencies above and below cutoff unlike the solution derived by Homicz and Lordi [4].

Each mode arriving at the duct open end radiates acoustic power with an efficiency that depends predominantly on how well it is cuton or cutoff, as shall be explored in Section 4. In this paper the modal radiation efficiency, τ_{mn}, is defined as the non-dimensional ratio of total radiated acoustic power W_{mn} to the power carried by the mean square axial velocity incident on the duct open end $\overline{u_{mn}^2} = \frac{1}{2}|U_{mn}|^2$,

$$\tau_{mn} = \frac{W_{mn}}{\rho_0 c_0 \frac{1}{2}|U_{mn}|^2\,S} \tag{11}$$

where ρ_0 is the mean density and c_0 is the ambient speed of sound.

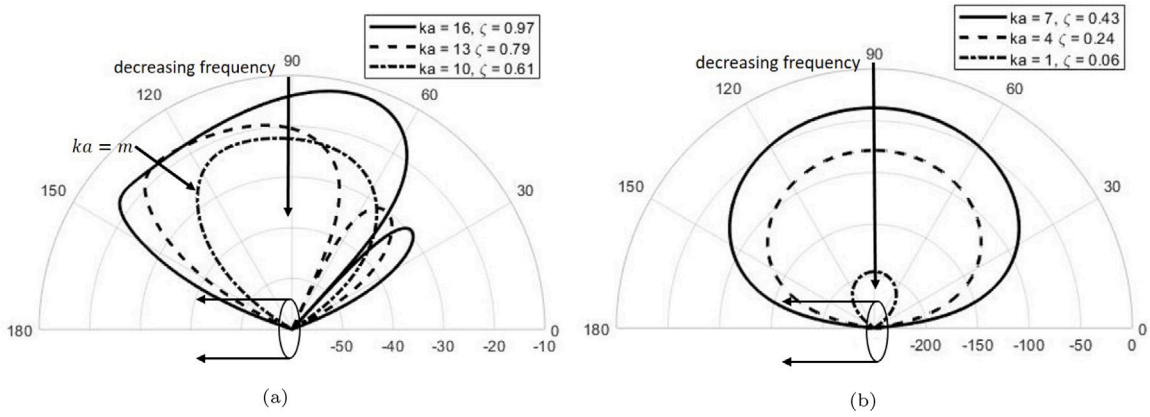

Fig. 2. Modal directivity for six frequencies between $ka = 16$ and 1. Plotted in decibels.

The radiated power W_{mn} can be determined by numerical integration of the far-field intensity, $W_{mn} = \int_S I_{mn}\, dS$,

$$W_{mn} = \frac{\pi}{\rho_0 c_0} R^2 \int_0^{\pi} |\hat{p}_{mn}(R, \phi, \theta)|^2 \sin\phi \, d\phi \, . \tag{12}$$

In this definition of τ_{mn}, the modal velocity amplitude that is incident at the open end of the duct can be related to the pressure amplitude by the momentum equation, which gives

$$U_{mn} = \frac{1}{\rho_0 c_0} \frac{k_{z,mn}}{k} P_{mn} \, . \tag{13}$$

Note that this definition of radiation efficiency is fundamentally different from that investigated by Morfey for flanged ducts [8], which was defined with respect to the modal velocity amplitude *following* reflection. In his investigation Morfey specified a single modal velocity component at the open end, which was then radiated to the far-field to compute the radiated sound power using the Kirchhoff approximation. This modal amplitude is therefore the velocity distribution that occurs once modal scattering has occurred at the open end. By contrast, in the present study relating to unflanged ducts, however, specifying a single modal velocity component at the open end is not possible as the solution is expressed in terms of the modal pressure amplitude incident upon the duct open end, i.e. *before* scattering has occurred. The modal radiation efficiencies investigated by Morfey and those in the present study therefore differ by a factor relating to the modal scattering coefficients at the open end. It is therefore not possible to compare them directly although, as we shall show in this paper, they share a number of common characteristics.

3. Directivity characteristics of cutoff modes

In this section the directivity function $D_{mn}(\phi, ka)$ of modes excited at frequencies below the cutoff frequencies is investigated for unflanged semi-infinite ducts. Whilst the characteristics of the directivity for cuton modes is well established (by for example Gabard and Astley [6]), a systematic study of its behaviour for cutoff modes remains to be performed.

3.1. Modal directivity of cutoff modes

Fig. 2 shows the modal directivity in decibels, $10\log_{10}(|D_{mn}(\phi, ka)|^2)$, for an arbitrary mode $(m, n) = (10,2)$, at six non-dimensional frequencies ka between 1 and 16, for which the mode is cutoff with modal cutoff ratios equal to $\zeta = 0.97, 0.79, 0.61, 0.43, 0.24$ and 0.06.

The six modal directivities under investigation, for which the modes are cutoff, have been divided into two groups. The first, plotted in Fig. 2(a), represent frequencies for which $\xi_m > 1$, while those on the right in Fig. 2(b) are at frequencies corresponding to $\xi_m < 1$. Distinct differences in behaviour can be observed between the two groups.

The directivity patterns in Fig. 2(a) are of roughly the same level and characterised by a number of sidelobes. The most striking feature of these directivities is that the main radiation lobe can be directed towards the rear-arc. This behaviour is contrary to the behaviour of cuton modes.

For a mode just below cutoff, the main radiation lobe can be observed in the forward-arc near $\phi = 90°$. As the mode becomes more cutoff the region of largest directivity can be observed in the rear-arc radiation to move towards the sideline direction $\phi = 90°$ as the frequency is reduced below cutoff. These behaviours will be explored in further detail in Section 3.2.

In Fig. 2(b), the modal directivities at the frequencies for which $\xi_m < 1$ can be observed to exhibit very different behaviours. The most striking feature is the absence of sidelobes with a main radiation lobe directed close to $\phi = 90°$. Fig. 2(b) also indicates that modes excited in the range $\xi_m < 1$ exhibit forward and rear-arc symmetry. However, the main feature of this figure is the

significant level of reduction with decreasing frequency below cutoff. The frequency $\xi_m = 1$ therefore marks the transition between the presence of sidelobes for $\xi_m > 1$ and the case when no sidelobes are present.

For both cuton and cutoff modes the location of the nulls are at angles given by Eq. (15). Following the 'interlacing' property of the Bessel function (Chapman [14]), the angular location of the main lobe of a given radial order n corresponds to the same location for the nulls of a different radial order n', for two modes of the same azimuthal order m.

The angular location ϕ_{mn} of the nulls in the far-field directivity are associated with the angles for which the Kernel function $K_m^+(\cos\phi_{mn})$ in the denominator of the directivity function of Eq. (10) tends to infinity. Inspection of Eqs. (A.2) and (A.4) shows that this occurs where

$$J'_m(ka\sin\phi_{mn}) = 0\,. \tag{14}$$

Eq. (14) for the angular location of the directivity nulls is satisfied at angular locations

$$\phi_{mn} = \sin^{-1}(1/\zeta_{mn})\,. \tag{15}$$

For cuton modes $\zeta_{mn} > 1$, and hence $0° \le \phi_{mn} \le 90°$. By contrast, cutoff modes are characterised by $\zeta_{mn} < 1$, and hence no real solutions exists for ϕ_{mn}. Sidelobes are therefore absent in the rear-arc and can only exist in the forward-arc.

Another feature of these directivity functions, which are also observed in Fig. 2, is the presence of a range of angles of very weak radiation close to the duct axis, which are identical in the front and rear-arcs in Fig. 2. These are commonly referred to as the 'quiet zone'. Chapman [14] has investigated in detail the characteristics of this zone and provides a physical interpretation for the reason why the angle of the quiet zone ϕ_m is independent of radial mode order and is given by,

$$\phi_m = \sin^{-1}(1/\xi_m). \tag{16}$$

The angle of the quiet zone of Eq. (16) is particularly important for cutoff modes since it is shown later in Fig. 3 that it closely corresponds to the angle of maximum radiation in the rear-arc.

Chapman provides a physical argument of Eq. (16) for the quiet zone based on the circumferential phase speed c_θ of the mode, given by $\omega a/m$ [14], which is independent of the radial mode order. It is well established that the angle of maximum radiation occurs when the phase speed in the direction of the observer is sonic. Chapman demonstrates that this polar angle for a far-field observer, which delineates the transition between subsonic and supersonic phase speeds, and hence efficient and inefficient radiation, occurs at the quiet zone angle ϕ_m given above in Eq. (16).

3.2. Angle of maximum radiation for cutoff modes

In this section we explore the relationship between the angle of maximum radiation for cutoff modes and the modal cutoff ratios ζ_{mn} and ξ_m, which are shown to govern the location of the quiet zone.

The angle of maximum radiation is presented in Fig. 3 for three modes with azimuthal orders $m = 0, 1$ and 2, each with the same radial order $n = 10$. The angles are plotted against ζ_{mn} by varying frequency from below cutoff, $\zeta_{mn} \approx 0$, to above cutoff, $\zeta_{mn} = 1.2$.

Also plotted in this figure for cutoff modes, $\zeta_{mn} < 1$, is the curve $\sin^{-1}(1/\xi_m)$ (shown in red) representing the quiet zone angle, and for cuton modes $\zeta_{mn} > 1$, the curve $\sin^{-1}(1/\zeta_{mn})$ for the main radiation lobe angle. The angle of maximum radiation can be clearly seen to closely match the quiet zone angle for cutoff modes, whose level of agreement can be observed to improve as ka is increased, and the mode becomes less cutoff. As the frequency is increased towards the cuton frequency, $\zeta_{mn} \to 1$, the angle of maximum radiation tends to 180°. At frequencies just below cutoff, $\zeta_{mn} \approx 0.95$, the angle of maximum radiation shifts towards the sideline direction at 90°. At frequencies above the cutoff frequency, $\zeta_{mn} > 1$, the angle of maximum radiation then shifts towards the forward-arc and closely follows the angle $\sin^{-1}(1/\zeta_{mn})$. This figure makes clear that cutoff modes contribute most significantly to the radiation in the rear-arc and is determined solely by the azimuthal mode order m. By contrast, cuton modes radiate most strongly in the forward-arc whose angle of maximum radiation is determined by both m and n through the cutoff ratio.

To illustrate this general behaviour some representative directivity plots for mode $(m, n) = (1, 10)$ are included with $\zeta_{mn} = 0.01$ (well below cutoff), $\zeta_{mn} = 0.95$ (just below cutoff), and $\zeta_{mn} = 1.05$ (just above cutoff). These directivity plots highlight the sudden transition between the angle of maximum radiation in the rear-arc for the mode just below cutoff to the forward-arc just above cutoff. Finally, it is noted that the angle of maximum radiation is always at $\phi = 180°$ for the axi-symmetric, cutoff, $m = 0$ modes, consistent with Eq. (16).

3.3. Scaling law for the directivity of cutoff modes

Another feature of the modal directivity function of cutoff modes that distinguishes it from cuton modes is that it has no explicit dependence on the radial order n inasmuch that the shape of the directivity function only depends on the azimuthal order m. This behaviour is evident from the form of the directivity function of Eq. (10). Further analysis of this function is presented in Appendix which demonstrates that for modes with the same azimuthal order m, excited at the same frequency, the magnitude of the directivity varies as

$$D_{mn}(\phi, ka) \propto \frac{1}{\sqrt{\kappa_{mn} a}}\,, \tag{17}$$

for fixed m and ka.

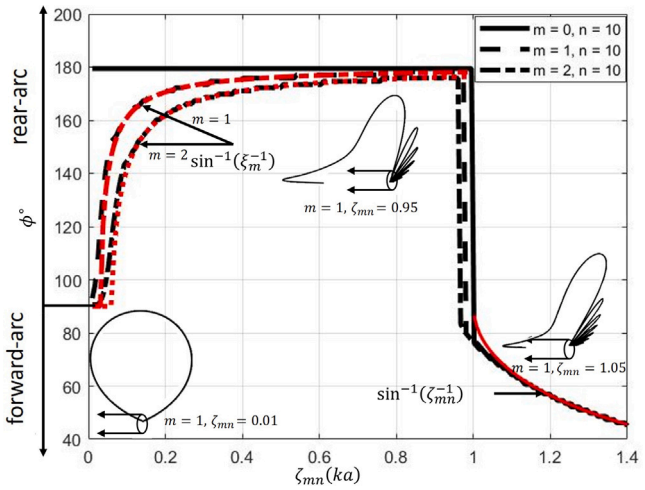

Fig. 3. Angle of the major lobe plotted against ζ_{mn} for modes (m,n) = (0,10) (1,10) (2,10). The curve in red for $\zeta_{mn} > 1$ represents $\sin^{-1}(1/\zeta_{mn})$ and for $\zeta_{mn} < 1$ is the shadow zone region ϕ_m, $sin^{-1}\xi_{mn}$ for the azimuthal orders $m = 1$ and 2. The directivity of the mode (m,n) = (1,10) is shown at three frequencies corresponding to $\zeta_{mn} = 1.05, 0.95$ and 0.01.

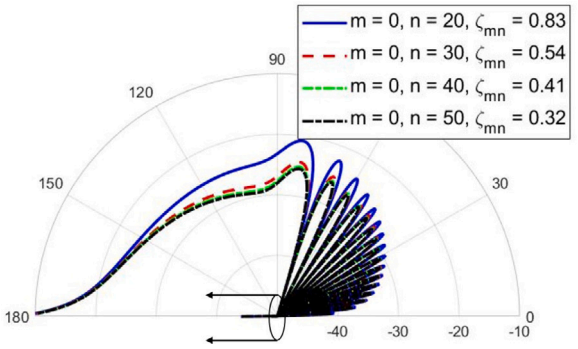

Fig. 4. Polar directivity factor $|D_{mn}(\phi, ka)|^2/\zeta_{mn}$ for four modes with azimuthal order $m = 0$ and radial orders $n = 20, 30, 40$ and 50, at $ka = 50$. Plotted in decibels.

Consequently, the radiation efficiency, discussed in Section 4, must vary as $1/\kappa_{mn}$ for fixed m and ka. For cutoff modes, the shape of the modal directivity only depends on m and ka, but for fixed m, the magnitude of the directivity is only dependent on $\kappa_{mn}a$. A clear demonstration of this phenomenon is shown in Fig. 4 which compares the square of the directivity function scaled by the inverse of the cutoff ratio, $|D_{mn}(\phi, ka)|^2/\zeta_{mn}$, plotted in decibels. The comparisons are shown for four cutoff modes with the same azimuthal order $m = 0$ and $ka = 50$, but with the different radial orders $n = 20, 30, 40$ and 50, corresponding to cutoff ratio ζ_{mn} of 0.83, 0.54, 0.41 and 0.32.

Excellent agreement is obtained for the three most well cutoff modes $\zeta_{mn} = 0.32, 0.41$ and 0.54, but with poorer agreement observed for the mode $\zeta_{mn} = 0.83$ that is closer to cuton, thereby confirming the relationship in Eq. (17).

4. Radiation efficiency of cutoff modes

In this section, the radiation efficiencies of cutoff modes is investigated. Radiation efficiency for cutoff modes was first investigated by Morfey [8] for flanged ducts, which included the effect on radiation due to a centrebody. In this paper the exact solution given by Eq. (10) for an unflanged duct is used to compute the radiation efficiency defined by Eq. (11). Morfey's main result was to show that the frequency dependence of the radiation efficiency of cutoff modes varies as

$$\tau_{mn} \propto (ka)^{2m+2}, \qquad |m| > 0\,, \tag{18}$$

which only depends on the azimuthal order m. No physical explanation was provided in this early paper, or any limit of the frequency range over which this result is valid.

As mentioned in the introduction it is not possible to compare directly the efficiencies of the flanged and unflanged solutions, as the former investigated by Morfey is based on the modal velocity amplitudes at the end of the duct *following* reflection, while in the current investigation the modal velocity amplitude is that of the incident mode *before* reflection has occurred at the open

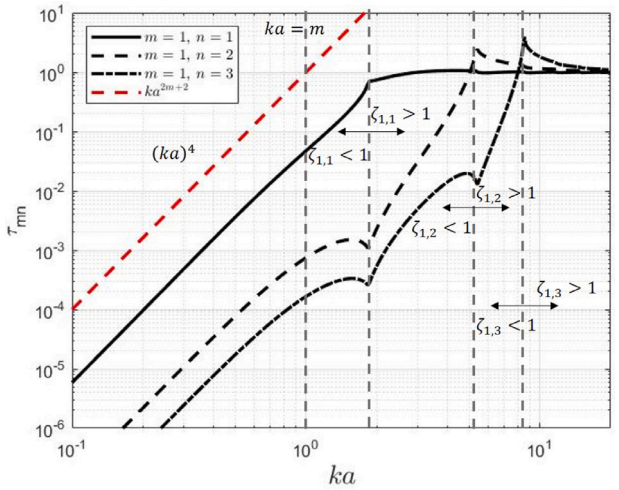

Fig. 5. Modal efficiency for azimuthal order $m = 1$, and radial order $n = 1, 2$ and 3.

end. However, this difference is not anticipated to affect the main frequency dependence identified by Morfey, but only affect the magnitude.

Fig. 5 shows the radiation efficiency τ_{mn} plotted against ka, computed from Eqs. (9)–(11). Fig. 5 shows results for radial orders $n = 1, 2$ and 3 with the same azimuthal order $m = 1$. Also shown in the figure is a plot of $(ka)^{2m+2}$ evaluated for $m = 1$.

Fig. 5 mostly confirms the prediction made by Morfey that the overall trend of the radiation efficiencies varies with frequency as $\tau_{mn} \propto (ka)^{2m+2}$. The general trend in the variation of radiation efficiency with frequency of these cutoff modes is therefore predominantly independent of n. However, it is observed that Morfey's result begins to deviate from the exact behaviour at frequencies $\xi_m > 1$. Following the analysis from Section 3.1, Morfey's result is therefore confined to the frequency range where sidelobes are completely absent, such as for those shown in Fig. 2(b), which are all excited at $\xi_m < 1$. This behaviour will be investigated further in Section 4 for modes excited in this region, where the strongest radiating velocity components are from outside the duct, which explains the low radiation efficiency.

Similar to Morfey, in this new work it is observed that maximum radiation efficiency occurs at cutoff $\zeta_{mn} = 1$, where τ_{mn} slightly exceeds unity, since it is not a true measure of energy efficiency. However, a number of features not apparent in Morfey's results are observed, principally the appearance of a number of peaks and dips. For the mode (m, n) these may be shown to occur at the cutoff frequencies of (m, n'), where $n' < n$. The radiation efficiency of the $(m, n)^{th}$ mode therefore has $(n-1)$ dips, where the radiation efficiency is relatively poor. This phenomenon can be attributed to peaks in the reflection coefficient at these frequencies cased by strong scattering of the mode (m, n) into (m, n') modes at their cutoff frequencies.

The general result of Eq. (18) has been found to provide a good fit to the frequency dependence of τ_{mn} for nearly all azimuthal orders m for modes excited below their cutoff frequency. A physical explanation for this finding will be presented in Section 5. However, Eq. (18) breaks down for the axi-symmetric $m = 0$ modes, which may be shown to have the same radiation efficiency as the $m = 1$ mode, and hence vary as $\tau_{mn} \propto (ka)^4$. This behaviour is also discussed in Section 5.

4.1. Sound power split between forward and rear-arcs

It is shown in Figs. 2–4 that cutoff modes radiate significantly to the rear-arc. In this section, the division in the total radiated sound power between the forward and rear-arcs is investigated in more detail.

The power split ratio η_{mn} is defined as the ratio between the sound power radiated to the forward-arc $0 \le \phi \le \pi/2$ to the total power radiated defined in Eq. (12). The ratio of sound power radiated to the rear-arc is therefore $1 - \eta_{mn}$.

Fig. 6(a) shows the power split ratio η_{mn} plotted against ζ_{mn} computed for the modes of constant radial order $n = 1$, and azimuthal order $m = 1, 2$ and 3. Fig. 6(b) shows the corresponding result for modes of constant azimuthal order $m = 1$ with $n = 1, 2$ and 3. In Fig. 6(b) the cutoff frequencies for modes of lower radial order are identified to highlight the significant behaviour observed for modes at that frequency. Appearance of dips is consistent with the so-called power reflection/transformation coefficients presented by Snakowska and Jurkiewicz [15].

Both figures reveal the existence of well defined low frequency and high frequency asymptotes for which the power split ratio tends to 0.5 and 1.0 respectively. The low frequency asymptote is a direct consequence of the symmetry of the directivity function about $\phi = \pi/2$ in the lower frequency limit. The high frequency asymptote provides evidence that the degree of diffraction of the acoustic mode around the duct opening becomes progressively weaker, and sound increasingly beams directly in the forward-arc. We note that the transition between equal energy split between the forward and rear-arcs, $\eta_{mn} = 0.5$, and dominance in the forward-arc occurs close to the cutoff frequency $\zeta_{mn} = 1$.

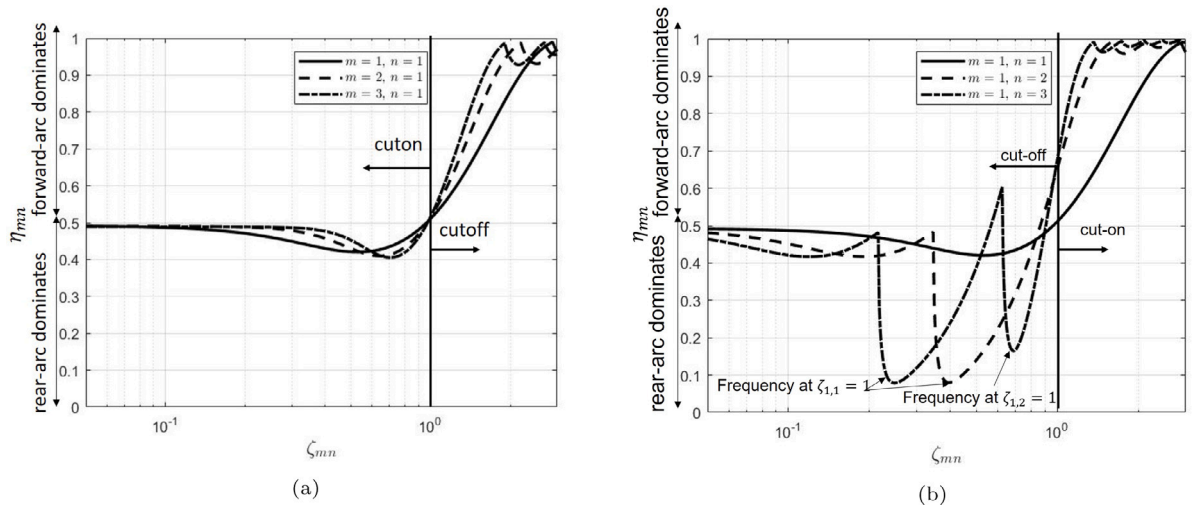

Fig. 6. Efficiency ratio comparing radiation efficiency in the forward-arc to the total radiation, (a) $m = 1, 2$ and 3 $n = 1$, (b) $m = 1$ and $n = 1, 2$ and 3.

In Fig. 6(b) showing the power split ratio for the different radial mode orders, distinct dips in η_{mn} can be observed, corresponding to frequencies at which the sound power is considerably greater in the rear-arc. These frequencies coincide with the cutoff frequencies of the lower radial orders $n' < n$. Reference to Fig. 5 indicates, therefore, that not only is the overall radiation efficiency τ_{mn} relatively weak at these frequencies, but its sound power is predominantly in the rear-arc.

5. Equivalent far-field source distribution

In this section we investigate the equivalent source distribution for cutoff modes in order to assist in the interpretation of the radiation characteristics presented above. By way of simplification we now introduce an infinite rigid flange onto the end of the duct. According to the Rayleigh integral the source distribution is now completely specified by the axial particle velocity everywhere at the exit plane $z = 0$ and is equal to zero on the flange $r > a$.

The radial variation of axial velocity for the $(m, n)^{\text{th}}$ mode incident at the exit plane of a flanged duct is given by,

$$u_{mn}(r) = \begin{cases} U_{mn}\,\psi_{mn}(r) & r \le a \\ 0 & r > a, \end{cases} \tag{19}$$

with a slight change in notation compared with Eq. (2). This is now decomposed into its wavenumber spectral components by use of the Hankel transform, i.e.

$$\widetilde{u}_{mn}(\kappa) = \int_0^\infty u_{mn}(r) J_m(\kappa r) r dr \tag{20}$$

where $\widetilde{u}_{mn}(\kappa)$ is the modal velocity wavenumber spectrum. Substituting Eq. (19) (and Eq. (2)) into Eq. (20), and replacing the upper limit of integration by $r = a$, gives the equivalent radiating velocity distribution. The integral can be evaluated analytically to give

$$\widetilde{u}_{mn}(\kappa) = U_{mn} \frac{\kappa a}{\kappa_{mn}^2 - \kappa^2} \frac{J_m'(\kappa a)}{\sqrt{\left(1 - \frac{m^2}{\kappa_{mn}^2 a^2}\right)}}. \tag{21}$$

The radial velocity distribution can be recovered from the spectrum by the inverse Hankel transform,

$$u_{mn}(r) = \int_0^\infty \widetilde{u}_{mn}(\kappa) J_m(\kappa r) \kappa d\kappa. \tag{22}$$

The dispersion relation in Eq. (5) suggests that the equivalent radiating velocity distribution $u_{mn}^{(r)}(r)$ is associated with the range of spectral wavenumber components in the range $0 < \kappa < k$, of the form

$$u_{mn}^{(r)}(r) = \int_0^k \widetilde{u}_{mn}(\kappa) J_m(\kappa r) \kappa d\kappa, \tag{23}$$

while non-radiating components are due to the high 'frequency' components of the spectrum $k < \kappa < \infty$.

5.1. Far-field radiation

The velocity components of Eq. (23) are now radiated. The radiation due to this equivalent perfectly radiating velocity distribution $u_{mn}^{(r)}(r)\,e^{-jm\theta}$ may be estimated by substituting Eq. (23) into the Rayleigh integral, from Tyler and Sofrin [2],

$$p_F^{(D)}(R,\phi,\theta,\omega) \approx \frac{jk\rho_0 c_0 e^{-jkR}}{2\pi R}\int_{S_0} u_z(r_0,\theta_0)e^{jkr_0\sin\phi\cos(\theta-\theta_0)}dS_0. \tag{24}$$

where r_0 and θ_0 are source elements on a vibrating surface inside a flange of cross sectional area S_0. Substituting Eq. (23) into (24), and solving the integral across θ_0 is solved using standard identities of the Bessel function,

$$p_{F,mn}(R,\phi,\theta) = j^{m+1}U_{mn}\rho_0 c_0 k\frac{e^{-j(kR+m\theta)}}{R}\int_0^k \widetilde{u}_{mn}(\kappa)\kappa\int_0^\infty J_m(\kappa r_0)J_m(kr_0\sin\phi)r_0 dr_0 d\kappa. \tag{25}$$

The integral over r_0 is evaluated using the orthogonality property of the Bessel function,

$$p_{F,mn}(R,\phi,\theta) = j^{m+1}U_{mn}\rho_0 c_0 k\frac{e^{-j(kR+m\theta)}}{R}\int_0^k \widetilde{u}_{mn}(\kappa)\left(\frac{\kappa}{k\sin\phi}\right)^{\frac{1}{2}}\delta(\kappa-k\sin\phi)d\kappa, \tag{26}$$

where $\delta(\cdot)$ is the Dirac-delta function. The sifting property of the delta function applied to the term $\delta(\kappa - k\sin\phi)$ implies that each spectral component κ radiates only to a single polar radiation angle $\phi = \sin^{-1}(\kappa/k)$, and is zero everywhere else. After integration over κ, and assuming that reflections can be neglected so that the velocity amplitude U_{mn} is assumed to be solely due to the incident mode with pressure amplitude P_{mn}, the expression for the far-field directivity may be directly related to the velocity wavenumber spectrum,

$$D_{F,mn}(\phi,ka) = j^{m+1}\frac{k_{z,mn}}{k}\frac{1}{U_{mn}}\widetilde{u}_{mn}(k\sin\phi). \tag{27}$$

Substituting $\kappa = k\sin\phi$ in Eq. (27) gives the classical solution deduced by Tyler and Sofrin [2], given by

$$D_{F,mn}(\phi,ka) = j^{m+1}\frac{k_{z,mn}}{k}\frac{\sin\phi J_m'(ka\sin\phi)}{(\frac{\kappa_{mn}^2}{k^2}-\sin^2\phi)\sqrt{\left(1-\frac{m^2}{\kappa_{mn}^2a^2}\right)}}, \tag{28}$$

which can be used to approximate the far-field pressure radiated from a duct in the forward-arc ($0 < \phi < 90°$) using Eq. (9). The velocity spectrum at $\kappa = k$ therefore radiates solely in the sideline direction at 90° to the duct axis, while $\kappa = 0$ radiates only on-axis at 0°.

5.2. Radiating velocity components of cutoff modes

We now use this theoretical framework to identify the essential differences between the radiation due to cuton and cutoff modes. Fig. 7 shows a plot of the modulus of the wavenumber velocity spectrum $\widetilde{u}_{mn}(\kappa)$, normalised to the maximum value, for a typical mode $(m,n) = (9,6)$ excited below its cutoff frequency $\zeta_{mn} = 0.8$, plotted against κ/κ_{mn}. The vertical line indicates the frequency of excitation $k/\kappa_{mn} = 0.8$. Clearly, the range of velocity components responsible for far-field radiation in the forward-arc $0° < \phi < 90°$ now lies below the peak in the spectrum at $\kappa = \kappa_{mn}$, and therefore radiation to the far-field is comparatively weak and absent of a main radiation lobe, as discussed above.

In this example, since the mode is excited below its cut-on frequency, and is therefore cutoff, the range of radiating wavenumbers κ therefore all occur below the cuton wavenumber $\kappa = \kappa_{mn}$. When the mode is excited exactly at the cuton frequency, therefore, the maximum radiating wavenumber component κ is therefore equal to the cuton wavenumber.

5.3. Radiating velocity distribution for cuton modes

First the radiating velocity distribution for three high-order cuton modes with the same azimuthal order $m = 10$ and radial orders $n = 1, 5$ and 10, excited at the same frequency corresponding to modal cutoff ratios $\zeta_{mn} = 4.24$, 1.84 and 1.15, is investigated. The velocity distributions are plotted in Fig. 8(a), b and c respectively.

The equivalent perfectly radiating velocity distribution can be observed to extend beyond the duct $r > a$. This is to be expected as its wavenumber spectrum from Eq. (20) is strictly band-limited in the wavenumber domain to $0 < \kappa < k$, which from elementary theory suggests that it must be unbounded in the space domain.

The equivalent radiating velocity distributions for these three cuton modes can be observed to closely match the mode shape functions $\Psi_{mn}(r,\theta)$ of Eq. (3). It is now shown by numerical example that the radial variation in the equivalent perfectly radiating velocity tends exactly to the mode shape function $\psi_{mn}(r)$ in the high frequency limit $k \to \infty$. Note that attempts to prove this formally from solutions of Eq. (23) for $k = \infty$ were unsuccessful. Integrals of this type do not appear to be included in classical treatise on Bessel functions such as Watson [16].

Fig. 9 shows a comparison of the result computed from Eq. (23) for the mode $(m,n) = (10,5)$ at the frequency of $\zeta_{mn} = 10$ with the exact mode shape function $\psi_{mn}(r)$. Note that both results have been normalised to their maximum value.

Near perfect agreement between the two curves is observed, with the greatest deviation occurring near the wall $r/a = 1$ where small rapidly decaying oscillations are present. Note that these oscillations become progressively smaller as the frequency is increased further. This figure provides clear evidence that in the high frequency limit the entire modal velocity radiates to the far-field, and this is the reason why the radiation efficiency tends to unity in the high-frequency limit.

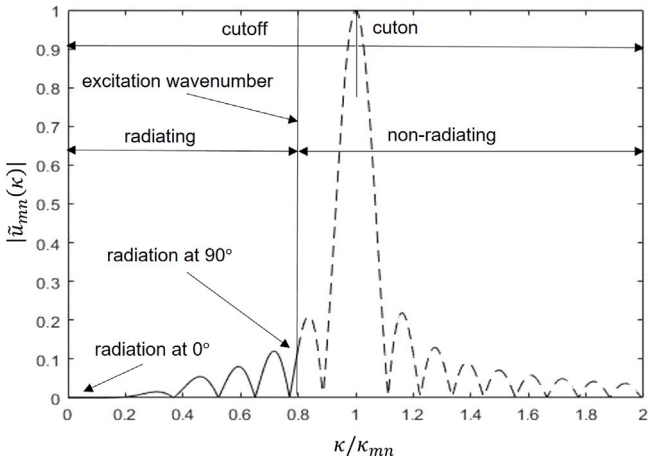

Fig. 7. Wavenumber spectrum for the cutoff mode $(m, n) = (9, 6)$, $\zeta_{mn} = 0.8$.

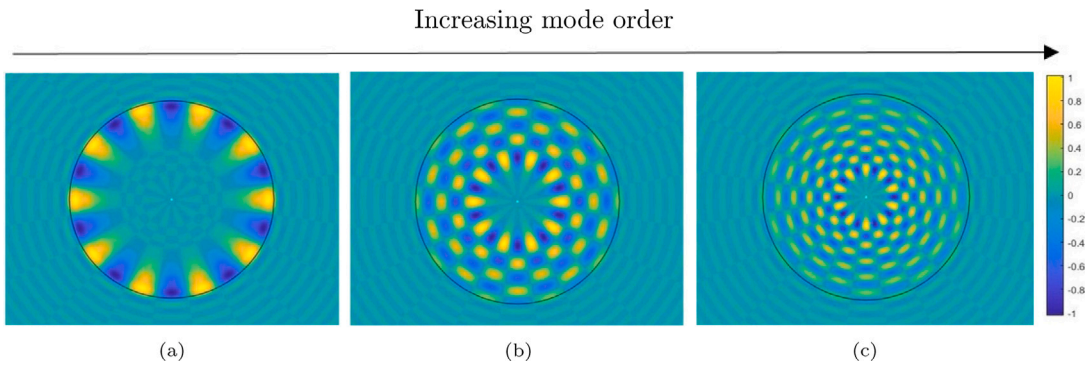

Fig. 8. Radiating velocity distribution at the open end of the duct for varying cuton modes. The duct is denoted by the black circle, (a) $ka = 50, m = 10, n = 1$, $\zeta_{mn} = 4.24$ (b) $ka = 50, m = 10, n = 5$, $\zeta_{mn} = 1.84$ (c) $ka = 50, m = 10, n = 10$, $\zeta_{mn} = 1.15$.

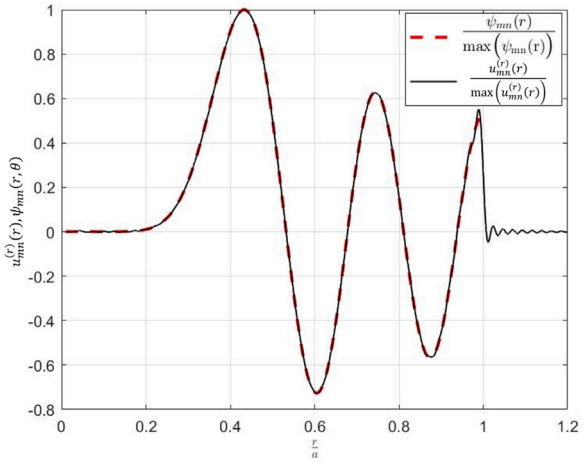

Fig. 9. Comparison between radial variation of radiating velocity distribution and mode shape function for the mode $(m, n) = (10, 5), \zeta_{mn} = 10$.

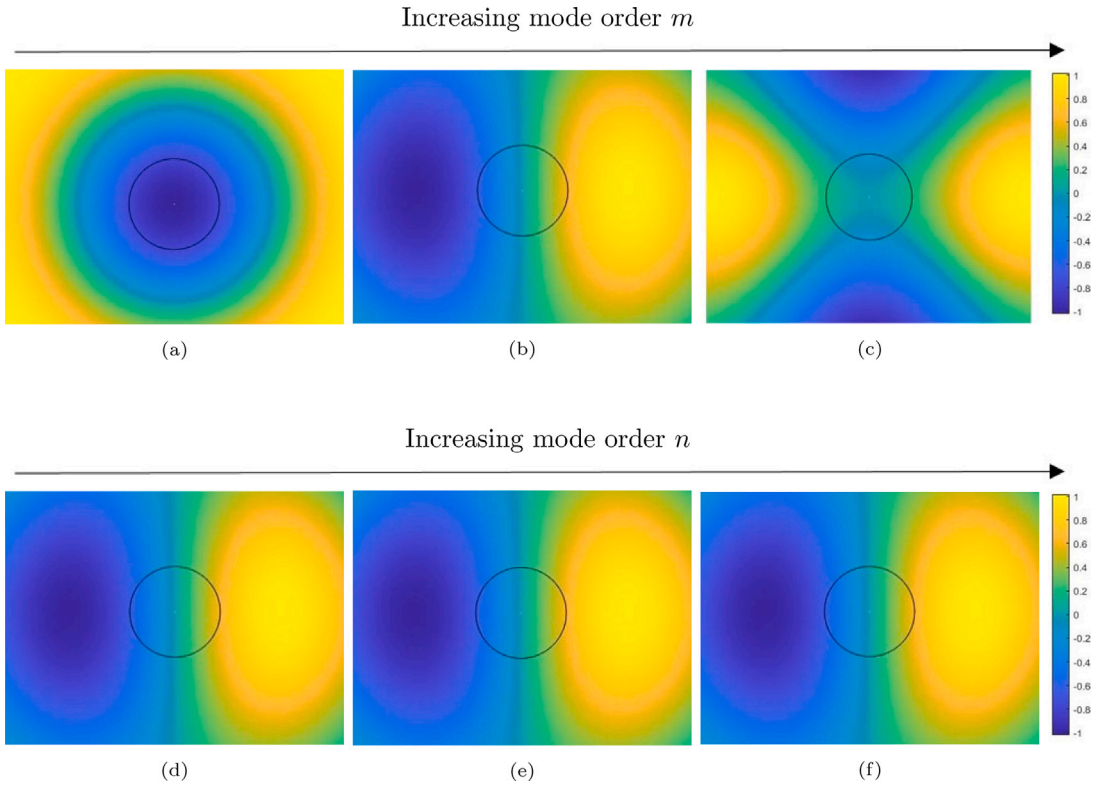

Fig. 10. Radiating velocity distribution at the open end of the duct for different modes. The duct is denoted by the black circle, (a) $ka = 1, m = 0, n = 2$, (b) $ka = 1, m = 1, n = 2$, (c) $ka = 1, m = 2, n = 2$, (d) $ka = 1, m = 1, n = 2$, (e) $ka = 1, m = 1, n = 3$, (f) $ka = 1, m = 1, n = 4$.

5.4. Radiating velocity distribution for cutoff modes

Eq. (23) is used to compute the equivalent radiating velocity, shown in Fig. 10, for three typical cutoff modes of different azimuthal order $m = 0, 1$ and 2, for the same radial order $n = 2$, and three typical cutoff modes of different radial order $n = 2, 3$ and 4, for the same azimuthal order $m = 1$, excited at the non-dimensional frequency $ka = 1$.

Fig. 10 shows that the equivalent velocity distribution is dominated by the azimuthal order m of the mode with no apparent dependence on n. These velocity distributions for $m = 1$ and 2 can be observed to have dipole and quadrupole type behaviours respectively, which explains their frequency dependencies of $(ka)^4$ and $(ka)^6$, which are well established results from classical radiation theory [17]. Clearly, the degree of destructive interference will increase with increasing m, and hence the reason for the reduction in radiation efficiency with increasing m.

Note that the velocity distribution for $m = 0$ is a special case for which the general formula by Morfey [8] $\tau_{mn} = (ka)^{2m+2}$ breaks down. A cutoff mode with $m = 0$ has the same frequency dependence as for $m = 1$ modes and therefore does not radiate with monopole type efficiency. This is evident from the velocity distribution of Fig. 10(a) which shows a concentric series of pressures of oscillating phase. These phase variations result in destructive interference leading to less efficient radiation than if the velocity was all radiating in phase. This velocity may therefore be interpreted as an 'azimuthal dipole'.

Fig. 10 shows clearly that the effective normalised radiating velocity distribution is independent of n. This behaviour helps provides further evidence that the behaviour of the radiation of cutoff modes is only weakly affected by the radial order n, and hence why their directivities and efficiencies are very similar.

5.5. Sonic radius

In this section the radiating velocity distributions for cuton and cutoff modes is contrasted, in order to highlight the fundamental difference in the radiation characteristics when the mode becomes cutoff. Previous sections in this paper have shown that, for cutoff modes, the radiation efficiency and modal directivity are predominantly governed by the azimuthal order m, with very weak dependence on the radial order n.

The expression for the equivalent perfectly radiating velocity distribution, after substituting Eq. (20) into Eq. (23) comprises three terms. However, only the third term $J_m(\kappa r)$ varies with radius r. The Bessel function $J_m(x)$ is known to exhibit exponential-type behaviour for $x < m$ with its first maxima at $x \approx m$. The equivalent radiating velocity distribution is therefore relatively small

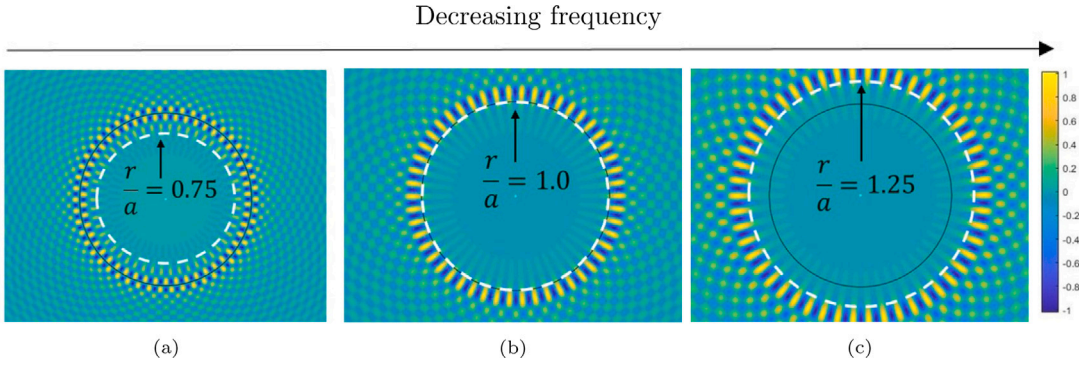

Fig. 11. Radiating velocity distribution at the open end of the duct for varying frequencies ka. The duct is denoted by the black circle, (a) $\xi_m^{-1} = 0.75, m = 50, n = 5$, (b) $\xi_m^{-1} = 1.0, m = 50, n = 5$, (c) $\xi_m^{-1} = 1.25, m = 50, n = 5$.

for $r/a < \xi_m$, peaking at $r = r_s$ and then oscillates at radial positions beyond this,

$$\frac{r_s}{a} \approx \xi_m^{-1}. \tag{29}$$

Demonstration of this behaviour is provided in Fig. 11, which shows plots of the equivalent velocity distribution computed from Eq. (23) for the high order cutoff mode $(m, n) = (50,5)$ excited at the three different frequencies corresponding to cutoff ratios $\zeta_{mn} = 0.90, 0.67$ and 0.54. Their corresponding values of ξ_m^{-1} are equal to 0.75, 1.00 and 1.25. In each plot the radial location $r/a = \xi_m^{-1}$ is indicated as a white dashed circle while the duct radius is indicated a solid black circle.

In the first example in Fig. 11(a), relating to the least cutoff mode, $\xi_m < 1$. In this case the radiating velocity distribution can be observed to be negligible for $r/a < 0.75$, and reaches its maximum value at the duct radius $r/a = 1$. The results from other calculations have shown to be generally true for all the cases for which $\xi_m \geq 1$. As the frequency is reduced, the mode becomes more cutoff. When the critical frequency is reached, $\xi_m = 1$, and the radiating velocity becomes negligible within the duct $r/a < 1$. At this frequency, the maximum velocity is observed at the duct radius $r/a = 1$, which coincides with the sonic radius $r_s/a = 1$. All three plots in Fig. 11 show the radiating velocity is outside the sonic circle. As the frequency is reduced further, the mode becomes increasingly cutoff, and significant radiating velocity now only occurs outside the sonic radius $r_s/a > 1$, and is negligible within it, according to Eq. (29).

In all examples presented in Fig. 11, $r/a = \xi_m^{-1}$ marks the transition radially between high and low velocity. This radial location is also shown by Eq. (29) to represent the location of the sonic radius, for which the azimuthal phase speed becomes sonic. At radii smaller than the sonic radius the azimuthal phase speed is subsonic and is therefore weakly radiating while at greater distances the phase is supersonic and is hence efficiently radiating. In the previous section, the radius r_s delineating the region of significant radiating velocity was identified from its maximum value. However, it is demonstrated that the radius r_s has a more fundamental physical interpretation as the sonic radius.

To establish this principle more clearly consider a point on the modal wavefront of constant phase $\chi(z, \theta, t)$, such that the mode propagates along the duct as $e^{j\chi(z,\theta,t)}$, where $\chi = k_{z,mn}z + m\theta - \omega t$. The azimuthal phase speed at a fixed radial and axial position r and z is given by $c_\theta(r) = r\partial\theta/\partial t$. Solving the expression for θ in the expression above for χ and differentiate with respect to time, the expression for the azimuthal phase speed becomes $c_\theta(r) = \omega r/m$. Classical radiation theory [17] dictates that radiation to the far-field can only occur if the phase speed in the direction of the observer exceeds the speed of sound. Only velocity components at radii r corresponding to $c_\theta(r) \geq c_0$ can therefore radiate. The transition between radiating and non-radiating components therefore occurs at the sonic radius at which the azimuthal phase speed equals the sound speed, which from the argument above is identical to Eq. (29) above obtained from the first maxima of the Bessel function $J_m(\kappa r)$. Eq. (29) therefore has the simple physical interpretation as the sonic radius, which is determined completely by m, providing further evidence for why many of the characteristics of cutoff modal radiation is predominantly only a function of the azimuthal order m, and which only has a negligible dependence on radial order n, except when excited close to their cuton frequencies.

5.6. Energy interpretation of the radial mode *n* weak dependencies for cutoff modes

Further insight into the dependence of the radiation directivity and efficiency for cutoff modes predominantly on m can be obtained by examining the behaviour of its sound intensity propagating towards the open end. The acoustic intensity $\boldsymbol{I}_{mn}(r, \theta, z)$, inside the duct, is given by

$$\boldsymbol{I}_{mn}(r, \theta, z) = \frac{1}{2} Re\{\hat{p}_{mn}(r, \theta, z, \omega)\hat{\boldsymbol{u}}_{mn}^*(r, \theta, z, \omega)\}, \tag{30}$$

where the incident particle velocity $\hat{\boldsymbol{u}}_{mn}$ is found via the momentum equation,

$$j\omega\rho_0\hat{\boldsymbol{u}} = \nabla\hat{p}. \tag{31}$$

Substituting Eq. (31) and Eq. (1) into Eq. (30) leads to an expression for the intensity of the form

$$\boldsymbol{I}_{mn}(r,\theta,\phi) = \left(\frac{m}{kr}\vec{\theta} - \frac{Re\{k_{z,mn}\}}{k}\vec{z}\right)\frac{|\hat{p}_{mn}(r,\theta,z)|^2}{2\rho_0 c_0}\,, \tag{32}$$

where $\vec{\theta}$ and $\vec{z}$ are unit vectors in the θ and z directions.

This result suggests that for cuton modes, $Re\{k_{z,mn}\} \neq 0$, have sound intensity has components in both azimuthal and axial directions. For cutoff modes, however, $Re\{k_{z,mn}\} = 0$ and hence sound intensity incident upon the open end is solely in the azimuthal direction. Radiation to the far-field is therefore only possible through the interaction of the incident field with the open end, which has the effect of altering the phase relationship between the acoustic pressure and particle velocity. The radiation directivity and associated efficiency must therefore be predominantly governed by the azimuthal mode index m as verified by Figs. 4 and 5.

Radiation efficiency intensity is dependent on both modal indices m and n, however for cutoff modes the axial wavenumber $k_{z,mn}$ is imaginary, which removes the axial component from the intensity. Physically this represents the power of cutoff modes rotating around the duct instead of propagating axially. The azimuthal dependence of cuton and cutoff modes varies as $\exp(-jm\theta)$ and does not depend on radial mode index n, therefore by extension the far-field directivity is also independent of n. However, Fig. 4 indicates that modes excited just below cutoff have a weak dependence on n, which is likely a result of the effect of reflection at the open end, which is a large effect for modes excited just below cutoff.

6. Conclusion

This paper presents an investigation on the radiation characteristics of cutoff modes, which appear to have received little attention in the open literature. The motivation for this study is the increasingly shorter ducts used in the aviation and marine industries, where the distance of the fan/rotor plane from the duct open end is relatively small compared to the acoustic wavelength.

A summary of the main findings are listed below:

1. Cutoff modes radiate most strongly to the rear-arc.
2. A cutoff mode exhibits a major lobe whose radiation angle is determined only by m. A number of side lobes are also present above a threshold frequency given by $ka > m$, ($\xi_{mn} > 1$).
3. The directivity of cutoff modes is roughly symmetric about 90° at sufficiently low frequencies with $ka < m$ ($\xi_{mn} < 1$). In the low frequency limit, the total sound power is equally distributed between the forward and rear-arcs.
4. For sufficiently well cutoff modes the radiation efficiency τ_{mn} is solely dependent on the azimuthal order m and has dependency $\tau_{mn} \propto (ka)^{2m+2}$.
5. The equivalent radiation velocity distribution for cutoff modes has been shown to be predominantly located beyond the sonic radius at which the azimuthal phase speed equals the speed of sound.
6. Whilst the behaviour of well cutoff modes is mainly governed by m, their sensitivity to the radial mode index n increases as the frequency approaches cuton from below. The transition from cutoff to cuton is therefore gradual.
7. At a fixed frequency and azimuthal order m, the directivity of cutoff modes has been shown to vary as $D_{mn}(\phi, ka) \propto \sqrt{1/\kappa_{mn}}$.

Declaration of competing interest

The authors declare that they have no known competing financial interests or personal relationships that could have appeared to influence the work reported in this paper.

Data availability

No data was used for the research described in the article.

Acknowledgements

Funding for this work was gratefully accepted by the Engineering and Physical Sciences research council, United Kingdom and the Defense Science and Technology Laboratory, United Kingdom. The authors would like to express gratitude to Gwenael Gabard for supplying the code to calculate the directivity patterns for the unflanged duct model.

Appendix. Derivation of scaling-law for cutoff modes

In this appendix, simple scaling laws are derived for the directivities $D_{mn}(\phi, ka)$ of cutoff modes in terms of their transverse wavenumber κ_{mn} for both unflanged and flanged ducts. It is shown that the directivities of cutoff modes exhibit a particularly simple dependence on κ_{mn}, but their behaviour for flanged and unflanged ducts is fundamentally different.

A.1. Scaling-law for unflanged ducts

The starting point for the scaling law analysis is the solution for cutoff modes radiated from an unflanged based. The directivity function (Eq. (10)) derived by Gabard and Astley [6] for a circular, unflanged duct is of the form,

$$D_{mn}(\phi, ka) = \frac{(1-\cos\phi)}{\pi ka \sin\phi H_m'(ka\sin\phi)} \frac{(ka + k_{z,mn}a)}{(k_{z,mn}a - ka\cos\phi)\sqrt{\left(1-\frac{m^2}{\kappa_{mn}^2 a^2}\right)}} \frac{K_m^-(\kappa_{mn}a)}{K_m^+(\cos\phi)}, \tag{A.1}$$

where K_m^+, K_m^- are the positive and negative Kernel functions arising from the Wiener–Hopf solution. The Kernel functions are given in the form,

$$K_m^{\pm}(\Theta) = e^{j\mathcal{K}_m(\Theta) \pm \frac{1}{2}K(\Theta)}, \tag{A.2}$$

where $\mathcal{K}_m$ is the complex phase factor,

$$\mathcal{K}_m(\Theta) = \frac{ka}{2\pi}\int_0^1 \left[\frac{K(ka\sqrt{1-v^2}) - K(\Theta)}{v-\Theta} - \frac{K(ka\sqrt{1-v^2}) - K(\Theta)}{v+\Theta}\right]\frac{dv}{d\eta}d\eta. \tag{A.3}$$

and $K(\Theta)$ is the function,

$$K(\Theta) = \ln\left[\frac{\Theta}{ka}\left(\frac{J_m(\Theta)}{J_m'(\Theta)} - \frac{H_m(\Theta)}{H_m'(\Theta)}\right)\right]. \tag{A.4}$$

Furthermore, v is the polynomial function,

$$v = \frac{\eta}{(1-\eta)^2} - 2\eta(1-\eta)^2 j. \tag{A.5}$$

The function $K(\Theta)$ is a complex function of frequency whose phase is assumed to be a continuous function and therefore 'unwrapped'. Note also that the second term in $K(\Theta)$ is singular at the turning points of $H_m'(\Theta)$, and following Gabard and Astley [6], can be computed from the approximation,

$$\frac{H_m(\Theta)}{H_m'(\Theta)} \approx \frac{-8\Theta + (1-4m^2)j}{3 + 4m^2 - 8\Theta j}. \tag{A.6}$$

The dependency of the directivity function D_{mn} on radial order n is now investigated. Consider Eq. (A.1) and neglect the terms that do not depend on n,

$$D_{mn}(ka, \phi) \propto \frac{(ka + k_{z,mn}a)}{(k_{z,mn}a - ka\cos\phi)\sqrt{\left(1-\frac{m^2}{\kappa_{mn}^2 a^2}\right)}} \times \frac{1}{\sqrt{\kappa_{mn}a}} \times \frac{e^{j\mathcal{K}_m(\kappa_{mn}a)}}{\sqrt{\frac{J_m(\kappa_{mn}a)}{J_m'(\kappa_{mn}a)} - \frac{H_m(\kappa_{mn}a)}{H_m'(\kappa_{mn}a)}}} \tag{A.7}$$

Eq. (A.7) is valid for both cuton and cutoff modes. For sufficiently well cutoff modes $ka < |k_{z,mn}a|$, thus the term $(k_{z,mn}a + ka)/(k_{z,mn}a - ka\cos\phi) \approx 1$, and $\sqrt{1 - m^2/\kappa_{mn}^2 a^2} \approx 1$, since $m/\kappa_{mn} < 1$. Finally, we note from numerical studies that as the mode becomes increasingly cutoff ($\zeta_{mn} < 0.5$) the second term in Eq. (A.7) also becomes increasing independent of the radial order n and only dependent on azimuthal order m and frequency. By writing

$$\gamma_m = \frac{e^{\mathcal{K}_m(\kappa_{mn}a)}}{\sqrt{\frac{J_m(\kappa_{mn}a)}{J_m'(\kappa_{mn}a)} - \frac{H_m(\kappa_{mn}a)}{H_m'(\kappa_{mn}a)}}}, \qquad \zeta_{mn} < 1, \tag{A.8}$$

numerical calculations show the value of γ_m is approximately independent of ka, and its smallest value $\gamma_m(ka) \approx 0.7$, which increases with m for sufficiently cutoff modes.

Incorporating the approximations above leads to the scaling law for the directivity of cutoff modes of the form

$$D_{mn}(\phi, ka) \propto \frac{1}{\sqrt{\kappa_{mn}a}}, \tag{A.9}$$

for constant azimuthal order m and non-dimensional frequency ka.

A.2. Scaling law for flanged ducts

Following a similar analysis applied to the expression for the directivity for radiation from a flanged duct, as that for the unflanged duct, ignoring all terms that are independent of radial order n, gives,

$$D_{F,mn}(\phi, ka) \propto \frac{k_{z,mn}a}{\left(\frac{(\kappa_{mn}a)^2}{(ka)^2} - \sin^2\phi\right)\sqrt{\left(1-\frac{m^2}{(\kappa_{mn}a)^2}\right)}}. \tag{A.10}$$

Assuming well cutoff modes such that $\kappa_{mn} \gg k$, and hence making the approximations $\kappa_{mn}^2/k^2 \gg \sin^2\phi$, $m/\kappa_{mn} < 1$ and $k_{z,mn} \approx j\kappa_{mn}$ in Eq. (A.10), gives the following approximate scaling law for the directivity of cutoff modes,

$$D_{F,mn}(\phi, ka) \propto \frac{1}{\kappa_{mn} a}\,, \tag{A.11}$$

for constant azimuthal order m and non-dimensional frequency ka.

It is noted that this is a fundamentally different scaling law from that of Eq. (A.9) deduced for unflanged ducts. However, it is important to recognise that reflections have been neglected in this derivation so that direct comparison with Eq. (A.9) for the unflanged solution is not possible.

References

[1] H. Levine, J. Schwinger, On the radiation of sound from an unflanged circular pipe, Phys. Rev. 73 (4) (1948) 383.
[2] J. Tyler, T. Sofrin, Axial Flow Compressor Noise Studies, Tech. Rep., SAE, 1962.
[3] A. Weinstein, The theory of diffraction and the factorization method: Generalized Wiener-hopf technique, 1969.
[4] G. Homicz, J. Lordi, A note on the radiative directivity patterns of duct acoustic modes, J. Sound Vib. 41 (3) (1975) 283–290.
[5] R. Munt, The interaction of sound with a subsonic jet issuing from a semi-infinite cylindrical pipe, J. Fluid Mech. 83 (4) (1977) 609–640.
[6] G. Gabard, R. Astley, Theoretical model for sound radiation from annular jet pipes: Far-and near-field solutions, J. Fluid Mech. 549 (2006) 315–341.
[7] A. Snakowska, H. Idczak, B. Bogusz, Modal analysis of the acoustic field radiated from an unflanged cylindrical duct–theory and measurement, Acta Acust. United Acust. 82 (2) (1996) 201–206.
[8] C. Morfey, A note on the radiation efficiency of acoustic duct modes, J. Sound Vib. 9 (3) (1969) 367–372.
[9] E. Doak, Excitation, transmission and radiation of sound from source distributions in hard-walled ducts of finite length (II): The effects of duct length, J. Sound Vib. 31 (2) (1973) 137–174.
[10] K. Wang, T. Tszeng, Propagation and radiation of sound in a finite length duct, J. Sound Vib. 93 (1) (1984) 57–79.
[11] A. Snakowska, J. Jurkiewicz, A new approach to the theory of acoustic multi-port networks with multimode wave and its application to muffler analysis, J. Sound Vib. 490 (2021) 115722.
[12] M. Howe, Installation effects on the production of blade-vortex interaction noise by a ducted rotor, J. Sound Vib. 156 (1) (1992) 61–78.
[13] M. Goldstein, Aeroacoustics, Lewis Research Center, 1974.
[14] C. Chapman, Sound radiation from a cylindrical duct. Part 1. Ray structure of the duct modes and of the external field, J. Fluid Mech. 281 (1994) 293–311.
[15] A. Snakowska, J. Jurkiewicz, Efficiency of energy radiation from an unflanged cylindrical duct in case of multimode excitation, Acta Acust. United Acust. 96 (2010) 416–424.
[16] G. Watson, A Treatise on the Theory of Bessel Functions, Cambridge University Press, 1995.
[17] S. Rienstra, A. Hirschberg, An introduction to acoustics, Eindhoven Univ. Technol. 18 (2004) 249.